On Performance of Massive MIMO Systems with Solid-state Amplifiers

João Vítor C. Pessoa and Rafael S. Chaves

***Abstract*— This paper analyzes the impact of analog front-end nonlinearities on the *bit-error rate* (BER) performance of massive *multiple-input multiple-output* (MIMO) systems, mainly focusing on the *power amplifiers* (PAs) nonlinearities of the solid-state amplifier. Simulation results show that the PA nonlinearities degrade system BER, yielding SNR losses of approximately 2.3 dB to 5.1 dB depending on the number of user equipment, modulation order, and precoding or decoding schemes employed. The findings confirm the necessity of nonlinear compensation to guarantee the viability of massive MIMO in practical applications.**

***Keywords*— Massive MIMO, analog front-end, power amplifiers, BER.**

I. Introduction

Massive *multiple-input multiple-output* (MIMO) has been crucial for the technological advancement of mobile networks, enabling a wide range of innovative applications across various sectors by delivering high-speed and low-latency communications [1], [2]. Moreover, massive MIMO relies on simple linear precoding and decoding [3], effective power-control policies [4], [5], and in some situations user selection [6], [7]. Although it is a powerful technique, massive MIMO also introduces new challenges that must be studied to achieve a comprehensive understanding of its nature [8].

The deployment of massive MIMO systems necessitates large antenna arrays at the *base station* (BS), significantly increasing hardware costs. Although high-quality components improve system performance, they substantially raise expenses for BS and *user equipments* (UEs). Conversely, opting for lower-quality hardware introduces additional distortions due to the nonlinear behavior of analog front-end circuits, thereby degrading the system's *spectral efficiency* (SE) [9]. Such hardware impairments critically affect channel reciprocity, a key assumption for enabling efficient operations such as spatial multiplexing and beamforming. When reciprocity is compromised, channel estimation becomes less accurate, directly impairing the overall system performance [10].

One of the main sources of nonlinearity in massive MIMO systems comes from the *power amplifiers* (PAs), as well as *analog-to-digital* (AD) and *digital-to-analog* (DA) converters in the radio frequency chains [11]. These hardware imperfections introduce nonlinear distortions that reduce energy efficiency and significantly impair channel estimation accuracy and beamforming performance. Furthermore, high-order digital modulation schemes yield high *peak-to-average power ratio* (PAPR) signals, which are prone to hardware nonlinearity. This high-PAPR issue is particularly pronounced in *orthogonal frequency-division multiplexing* (OFDM) systems, commonly used in modern wireless communications due to their robustness against frequency-selective fading. In massive MIMO systems, which often leverage OFDM systems, high-PAPR signals remain a critical challenge [12]. These signals are especially susceptible to nonlinear distortions from PAs and AD/DA converters, exacerbating the degradation of spectral efficiency and further complicating accurate channel estimation and beamforming operations.

In the literature, several models have been proposed to characterize PA nonlinearities, including the Volterra series model [13], memory polynomial models [14], and Saleh's model [15], each offering different trade-offs between complexity and trustworthiness. These models are commonly used to assess the impact of nonlinearities on the SE and capacity of massive MIMO systems. Works investigating the influence of hardware impairments on system performance propose calibration techniques [16], distortion compensation strategies [17], and theoretical performance bounds for systems with hardware imperfections [18], [19]. However, this work departs from stochastic modeling by employing a deterministic, physically consistent PA model to enhance accuracy. This paper restricts the analysis to the nonlinear effects introduced by PAs, as they are typically the most dominant source of hardware-induced distortions in the transmission chain [20]. While AD and DA converters also contribute to system nonlinearities, their modeling often requires distinct treatment, involving quantization noise, which is beyond the scope of this study. Simulation results show that the PA nonlinearity degrades the BER performance, particularly with high-order modulation and large numbers of UEs scenarios. The system is robust to some nonlinearities in the downlink, yielding an SNR loss smaller than 0.3 dB at a BER of 10^{-3}. On the other hand, the system is sensitive to the nonlinearities in the uplink, yielding an SNR loss up to 6.5 dB at a BER of 10^{-5}.

The remainder of this work is structured as follows: Section II overviews massive MIMO fundamentals, detailing the system model. Section III presents the nonlinear amplifier model. Section IV presents simulation results and analysis. Finally, Section V concludes the paper and outlines directions for future research.

Notation: Vectors and matrices are represented by boldface lowercase and uppercase letters, respectively. The notation $\mathbf{X}^{\mathrm{T}}$, $\mathbf{X}^{*}$, and $\mathbf{X}^{\mathrm{H}}$ stand for transpose, complex conjugate, and Hermitian (conjugate transpose) operations on $\mathbf{X}$, respectively. $\mathsf{Diag}\,(\mathbf{x})$ is a diagonal matrix with $\mathbf{x}$ on its main diagonal. The symbols $\mathbb{C}$, $\mathbb{R}$, and $\mathbb{R}_{+}$ denote the sets of complex, real, and non-negative real numbers, respectively. The set $\mathbb{C}^{M\times K}$

João Vítor C. Pessoa and Rafael S. Chaves, Coordenação do Curso de Engenharia de Telecomunicações (CCGTEL), Centro Federal de Educação Tecnológica Celso Suckow da Fonseca (CEFET/RJ), Rio de Janeiro, RJ, Brazil, e-mails: joao.pessoa@aluno.cefet-rj.br and rafael.chaves@cefet-rj.br.

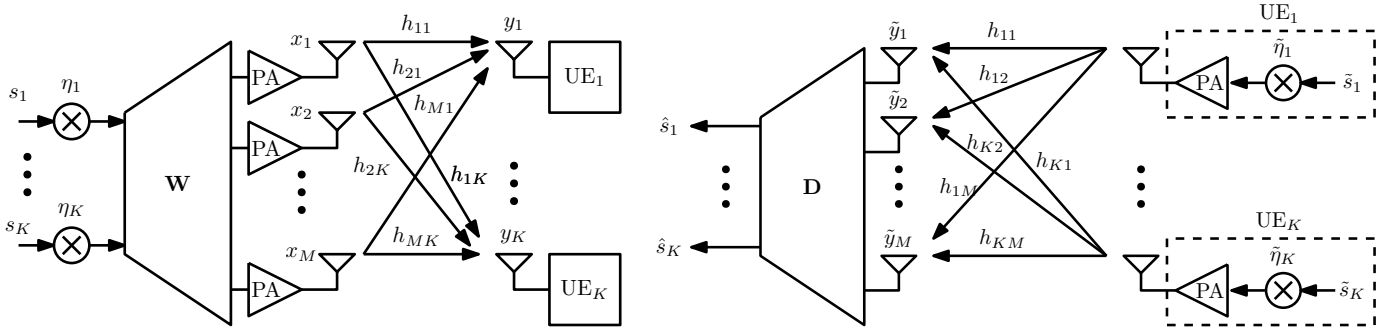

(a) Downlink. (b) Uplink.

Fig. 1: Signal model for massive MIMO considering the PA nonlinearity.

denotes all $M \times K$ matrices comprised of complex-valued entries. The symbol $\mathbf{I}_M$ denotes an $M \times M$ identity matrix and $\mathbf{0}_{M\times K}$ denotes an $M \times K$ zero matrix. The symbols $\mathcal{CN}(\mathbf{m}, \mathbf{C})$ and $\mathcal{U}(a, b)$ respectively denote a circularly symmetric Gaussian distribution with mean $\mathbf{m}$ and covariance matrix $\mathbf{C}$ and a uniform distribution between a and b. The notation $\mathbb{E}\{x\}$ stands for the expected value of x.

II. Massive MIMO System Model

Consider a generic single-cell massive MIMO system using *time-division duplex* (TDD) where K single-antenna UEs communicate with a BS equipped with M antennas. The system can operate in the downlink and the uplink. Additionally, the *power amplifier* (PA) nonlinearity is considered only in BS during the downlink and only in the K UEs during the uplink. Fig. 1 illustrates the massive MIMO transmission considering the PA nonlinearity operating in the downlink and uplink.

A. Downlink

In the downlink, the BS transmits the precoded signal given by

$$\mathbf{x} = \mathbf{W}\mathsf{Diag}\left(\boldsymbol{\eta}\right)^{1/2}\mathbf{s}, \tag{1}$$

where $\mathbf{s} \in \mathcal{C}^{K\times 1} \subset \mathbb{C}^{K\times 1}$ is the transmitted signal vector to the UEs, $\mathbf{W} \in \mathbb{C}^{M\times K}$ is the precoding matrix with normalized columns, and $\boldsymbol{\eta} \in \mathbb{R}_+^{K\times 1}$ is the downlink power allocation vector. Additionally, due to power limitations

$$\mathbb{E}\left\{\mathbf{x}^{\mathrm{H}}\mathbf{x}\right\} = 1. \tag{2}$$

The precoded signal is transmitted through the downlink channel and received by the UEs. The received signal by the UEs is

$$\begin{aligned}\mathbf{y} &= \sqrt{\rho}\,\mathbf{H}^{\mathrm{T}} f(\mathbf{x}) + \mathbf{v} \\ &= \sqrt{\rho}\,\mathbf{H}^{\mathrm{T}} f(\mathbf{W}\mathsf{Diag}\left(\boldsymbol{\eta}\right)^{1/2}\mathbf{s}) + \mathbf{v},\end{aligned} \tag{3}$$

where $f : \mathbb{C} \longrightarrow \mathbb{C}$ is the nonlinear model of the PAs at UEs, $\rho \in \mathbb{R}_+$ is the downlink SNR, $\mathbf{v} \sim \mathcal{CN}(\mathbf{0}_{M\times 1}, \mathbf{I}_M)$ is the additive white Gaussian noise (AWGN) at the UEs antennas, and $\mathbf{H}^{\mathrm{T}} \in \mathbb{C}^{M\times K}$ is the downlink channel matrix between the BS antenna array and the UEs.

It is worth highlighting that linear precoding algorithms are no longer optimal regarding spectral efficiency due to PA nonlinearity. Even with an ideal linear precoding and favorable propagation conditions, the PA nonlinearity impairs the transmitted signal estimate.

B. Uplink

In the uplink, the received signal at the BS is

$$\tilde{\mathbf{y}} = \sqrt{\tilde{\rho}}\,\mathbf{H} f(\mathsf{Diag}\left(\tilde{\boldsymbol{\eta}}\right)^{1/2}\tilde{\mathbf{s}}) + \tilde{\mathbf{v}}, \tag{4}$$

where $\tilde{\mathbf{s}} \in \mathcal{C}^{K\times 1} \subset \mathbb{C}^{K\times 1}$ is the transmitted signals by the UEs, $\tilde{\boldsymbol{\eta}} \in \mathbb{R}_+^{K\times 1}$ is the uplink power allocation vector, $\tilde{\rho} \in \mathbb{R}_+$ is the uplink SNR, $\tilde{\mathbf{v}} \sim \mathcal{CN}(\mathbf{0}_{M\times 1}, \mathbf{I}_M)$ is the AWGN at the BS antennas, and $\mathbf{H} \in \mathbb{C}^{M\times K}$ is the uplink channel matrix between the BS antenna array and the UEs. Moreover, the UEs transmit signals with unit power, meaning that

$$\mathbb{E}\left\{|\tilde{s}_k|^2\right\} = 1, \quad \forall\, k \in \mathcal{K}, \tag{5}$$

where $\mathcal{K} = \{1, 2, \cdots, K\}$ is the set of UE indices.

The BS decodes the received signal to recover an estimate of the transmitted signal. The estimate of the received signal can be expressed as

$$\begin{aligned}\hat{\mathbf{s}} &= \mathbf{D}\tilde{\mathbf{y}} \\ &= \sqrt{\tilde{\rho}}\,\mathbf{D}\mathbf{H} f(\mathsf{Diag}\left(\tilde{\boldsymbol{\eta}}\right)^{1/2}\tilde{\mathbf{s}}) + \mathbf{D}\tilde{\mathbf{v}},\end{aligned} \tag{6}$$

where $\mathbf{D} \in \mathbb{C}^{K\times M}$ is the linear decoding matrix with normalized columns.

C. Channel Model

The massive MIMO channel for the k-th UE can be written as

$$\mathbf{h}_k = \sqrt{\frac{\kappa}{\kappa+1}}\,\mathbf{h}_k^{\mathrm{LoS}} + \sqrt{\frac{1}{\kappa+1}}\,\mathbf{h}_k^{\mathrm{NLoS}}, \tag{7}$$

where $\mathbf{h}_k^{\mathrm{LoS}}$ represents the small-scale fading of the *line-of sight* (LoS) component, dependent on the geometry of the antenna array at the base station, $\mathbf{h}_k^{\mathrm{NLoS}} \sim \mathcal{CN}(\mathbf{0}, \beta_k\mathbf{I}_M)$ represents the small-scale fading of the *non line-of-sight* (NLoS) component, $\beta_k \in \mathbb{R}_+^{K\times 1}$ is the large-scale fading component, and $\kappa \in \mathbb{R}_+$ is the Rician factor that defines the ratio between the LoS and NLoS components [21]. In this work, the large-scale coefficient β_k [dB] is known at the BS and defined as [22]

$$\beta_k = -148 - 37.6\log_{10}\left(\frac{d_k}{1\text{ km}}\right), \tag{8}$$

where $d_k \in \mathbb{R}_+$ is the distance between the kth UE and the BS.

The channel model in (7) is the so-called uncorrelated Rician fading model, which considers the presence of both LoS and NLoS components. The LoS component depends on the BS antenna array steering vector. For an M-antenna *uniform linear array* (ULA), the LoS channel for the k-th user is given by

$$\mathbf{h}_k^{\text{LoS}} = \sqrt{\beta_k}\left[1 \quad \mathrm{e}^{\mathrm{j}\pi\sin(\theta_k)} \quad \cdots \quad \mathrm{e}^{\mathrm{j}\pi(M-1)\sin(\theta_k)}\right]^{\mathrm{T}}, \quad (9)$$

where $\theta_k \in \mathcal{U}(-\pi, \pi)$ is the angle-of-arrival for the k-th user.

III. Solid State Amplifier Model

In this work, the nonlinearities are assumed memoryless, an approximation valid for moderate bandwidths [23]. The analysis focuses exclusively on the influence of nonlinearities within the signal bandwidth, disregarding spectral regrowth. For a complex baseband input, the general relationship between the input and output of the nonlinearity $f : \mathbb{C} \longrightarrow \mathbb{C}$ can be expressed as

$$z = f(x) = f_A(|x|)\mathrm{e}^{\mathrm{j}(\phi + f_\phi(|x|)}, \quad (10)$$

where $|x| \in \mathbb{R}_+$ is the modulus of the baseband signal x, $\phi \in [-\pi, \pi]$ is the phase of the baseband signal x, $f_A : \mathbb{R}_+ \longrightarrow \mathbb{R}$ and $f_\phi : \mathbb{R}_+ \longrightarrow \mathbb{R}$ represent the *amplitude-to-amplitude* (AM-AM), and *amplitude-to-phase* (AM-PM) transfer functions, respectively.

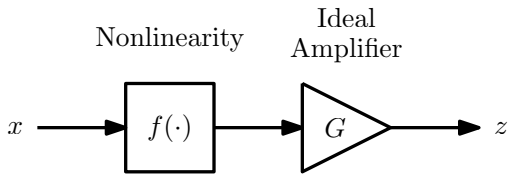

Fig. 2: Channel model with non-linear amplifier application.

Figure 2 shows the simplified model of a power amplifier considering the effect of nonlinearity. The input x initially is processed by a nonlinear function $f(\cdot)$, which introduces distortions or nonlinear effects typical of real power amplifiers. Then, the resulting signal is amplified by an ideal amplifier with gain G, yielding the output z. Considering the impact of nonlinearities in system modeling, it is essential to evaluate how they affect signal transmission in massive MIMO systems and capture the distortions generated by the hardware. This paper uses the solid-state amplifier, whose nonlinearity is only the AM-AM distortion given by [24]

$$f_A(|x|) = \frac{|x|}{\left(1 + \left[\frac{|x|}{A}\right]^{2p}\right)^{\frac{1}{2p}}}, \quad (11)$$

where $p > 0$ is an adjustment parameter that controls the smoothness of the nonlinear function, and $A \in \mathbb{R}_+$ is the saturation level. When p takes high values, the model converges to the ideal clipping amplifier with saturation level A. On the other hand, for low values of p, the transfer becomes smoother. Typically, p ranges from 1 to 3 [24]. It is worth highlighting that when $A \to \infty$, the PA becomes closer to the ideal amplifier.

TABLE I: Simulation Parameters

Parameters	**Value**
Number of antennas	$M = 256$
Number of UEs	$K \in \{64, 256\}$
Constellation	64-QAM and 256-QAM
Number of blocks	$N = 500$
Array geometry	ULA
Channel model	Rician Fading
Rician factor	$\kappa = 10$ dB
BS Power	10 W
UE Power	200 mW
BS and UEs Antenna Gain	0 dBi
Noise Figure	9 dB
Effective Downlink SNR	$\rho_{\text{dl}} \in \{-10, -5, \cdots, 30\}$ dB
Effective Uplink SNR	$\rho_{\text{ul}} \in \{-10, -5, \cdots, 30\}$ dB
Precoding algorithms	ZF and MMSE
Decoding algorithms	ZF and MMSE
Monte-Carlo (UEs position)	10
Monte-Carlo (Small-scale fading)	10

IV. Simulation Results

The performance is assessed via numerical simulations by evaluating the effect of the nonlinearity model presented in Section III on the BER and the constellation of the received signals for downlink and uplink. All the codes used in this work are available on GitHub.[1] The nonlinearity was evaluated with equal power allocation for different scenarios regarding the number of antennas and UEs with *zero-forcing* (ZF) and *minimum mean squared error* (MMSE) precoding and decoding algorithms.

A. Simulation Parameters

For the simulations, a 1000-radius hexagonal single-cell massive MIMO system with the BS equipped with a ULA with $M = 256$ antennas and $K \in \{64, 128, 256\}$ single-antenna UEs was used. The transmitter sent $N = 500$ blocks of a Q-QAM constellation with $Q \in \{64, 256\}$. The communication channel was Rician distributed with $\kappa = 10$ dB, and the carrier frequency was $f_{\text{c}} = 2$ GHz. The radiated power at the BS and the UEs were 10 W and 200 mW, the BS and UEs antenna gains were 0 dBi, and the noise figure was 9 dBi at both BS and UEs. With this configuration, a UE at the cell edge has the following equivalent downlink and uplink SNRs

$$\rho_{\text{dl}} = \rho\beta = 132 \text{ dB} - 148 \text{ dB} = -16 \text{ dB}, \quad (12)$$

$$\rho_{\text{ul}} = \tilde{\rho}\beta = 115 \text{ dB} - 148 \text{ dB} = -33 \text{ dB}. \quad (13)$$

Thus, in the simulations for both downlink and uplink, the BER was evaluated for $\rho_{\text{dl}},\ \rho_{\text{ul}} \in \{-10, -5, \cdots, 30\}$ dB. The BER was calculated using 10 realizations of UE positions, i.e., LoS channel, and for each UE position setup, 10 realizations of the small-scale fading were generated. Table I summarizes all the key parameters used in the simulations.

B. Bit-error Rate Performance

This subsection analyzed the downlink and uplink BER for varying SNR, considered perfect *channel state information*

[1] https://github.com/joaovcpessoa/massive_mimo_afe_impact

(CSI) knowledge, and a 64-QAM constellation. Fig. 3 shows the uplink BER *versus* SNR for $K \in \{64, 128, 256\}$, $A \in \{\text{Ideal}, 1, 2\}$, and ZF and MMSE decoders. One can observe in Figs. 3a and 3b that the BER degrades as expected with increasing K. The different decoders perform similarly, with the main difference being for the case of $K = 256$, where the MMSE decoder yields an SNR gain of ~ 15.8 dB at a BER of 10^{-1}. Moreover, one can observe a significant sensitivity to the PA saturation level, as for $A = 1$, the BER degrades substantially, regardless of the value of K and the decoding algorithm. For $A = 2$ and $K = 64$, the BER is worse than the BER for the ideal PA, yielding an SNR loss of ~ 6 dB and ~ 6.3 dB at a BER of 10^{-5} for ZF and MMSE decoders. On the other hand, for $K = 128$, the nonlinearity with $A = 2$ yields an SNR loss of ~ 6.5 dB and ~ 6.1 dB at a BER of 10^{-5} for ZF and MMSE decoders. These results indicate that for cases with $M >> K$ and a high saturation level, the PA nonlinearity impact on the BER does not scale with the number of UEs K.

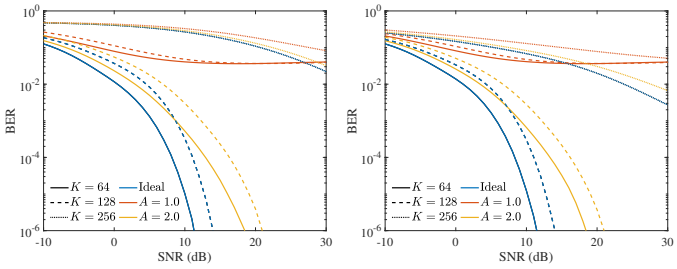

(a) ZF. (b) MMSE.

Fig. 3: Uplink BER *versus* SNR for $K \in \{64, 128, 256\}$, $A \in \{\text{Ideal}, 1, 2\}$, and ZF and MMSE decoders.

Fig. 4 illustrates the downlink BER versus SNR for $K \in \{64, 128, 256\}$, $A \in \{\text{Ideal}, 0.5, 1\}$, and ZF and MMSE decoders. Similar to the uplink, one can observe in Figs. 3a and 3b that different precoders do not yield any major difference in the BER, unless the case with $K = 256$, where the MMSE precoder improves the performance when the nonlinearity is considered. Regarding the impact of the nonlinearity on the BER, the downlink exhibits reduced sensitivity to PA nonlinearities due to the power allocation and the high number of antennas. For a saturation level of $A = 1$ and $M < K$, the nonlinearity slightly hinders the BER for both ZF and MMSE precoders, yielding an SNR loss smaller than 0.3 dB at a BER of 10^{-3}. On the other hand, for a stronger nonlinearity with $A = 0.5$, the precoders achieve an SNR loss lower than 0.7 dB and 3.2 dB at a BER of 10^{-3} for $K = 64$ and $K = 128$, respectively.

C. Nonlinearity Effects on the Constellation

This subsection evaluates the impact of the PA nonlinearity on the decoded signal constellation in the uplink. Fig. 5 shows the decoded signal constellation at the BS for 64 and 128-QAM modulations and $A \in \{\text{Ideal}, 0.5, 1.0, 2.0\}$. The SNR was fixed in 30 dB for the simulations since we aimed to evaluate solely the PA nonlinearity impact. One can observe

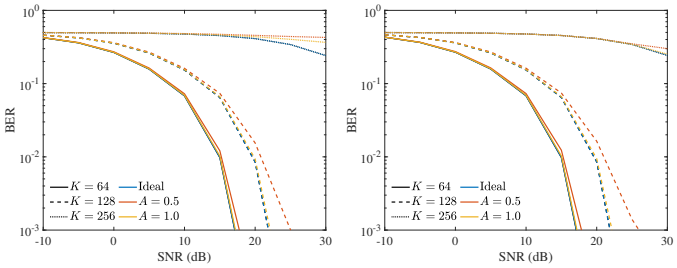

(a) ZF. (b) MMSE.

Fig. 4: Downlink BER *versus* SNR for $K \in \{64, 128, 256\}$, $A \in \{\text{Ideal}, 0.5, 1\}$, and ZF and MMSE precoders.

in the figure that the decoded signal is attenuated in amplitude and does not have any phase shift, which is expected because the SSA has an AM-AM transfer function; for both constellation sizes, decreased A yields more distortion in symbols close to the vertices of the constellation, placing the symbols in a circle. The symbols in the vertices are more susceptible to the effect of the nonlinearity because they have a higher amplitude. It is worth highlighting that the symbols close to the constellation center suffer from the PA nonlinearity, though they are not close to the saturation level.

V. Conclusion

This paper comprehensively analyzed the bit-error performance of massive MIMO systems with a solid-state amplifier, including a mathematical system description when the PA nonlinearity is included. Simulation results measured the impact of the PA nonlinearity in terms of SNR loss. The results showed that linear signal processing for precoding and decoding was not able to estimate the signals properly, albeit there were cases, mainly in the downlink, where the linear precoding yielded similar results to the ideal PA. Future works may explore the integration of nonlinear channel estimation techniques and the design of machine learning-based precoders and decoders to mitigate the impact of the observed nonlinearities. In particular, some deep learning models have shown promise in learning complex nonlinear mappings and can be employed to approximate optimal precoding and detection strategies in the presence of PA distortions and channel estimation errors.

Aknowledgements

This study was financed by FAPERJ - Fundação de Amparo à Pesquisa do Estado do Rio de Janeiro, Projeto FAPERJ E-26/210.157/2023. The Brazilian Research Councils CAPES and CNPq have also supported this work.

References

[1] O. Edfors, L. Liu, F. Tufvesson, N. Kundargi, and K. Nieman, *Signal Processing for 5G: Algorithms and Implementations*, pp. 189–230. PublisherJohn Wiley & Sons Inc., Aug. 2016.

[2] Y. Huo, X. Lin, B. Di, H. Zhang, F. J. L. Hernando, A. S. Tan, S. Mumtaz, Özlem Tuğfe Demir, and K. Chen-Hu, "Technology Trends for Massive MIMO towards 6G," 2023.

[3] T. L. Marzetta, "Noncooperative Cellular Wireless with Unlimited Numbers of Base Station Antennas," *IEEE Trans. Wirel. Commun.*, vol. 9, pp. 3590–3600, Nov. 2010.

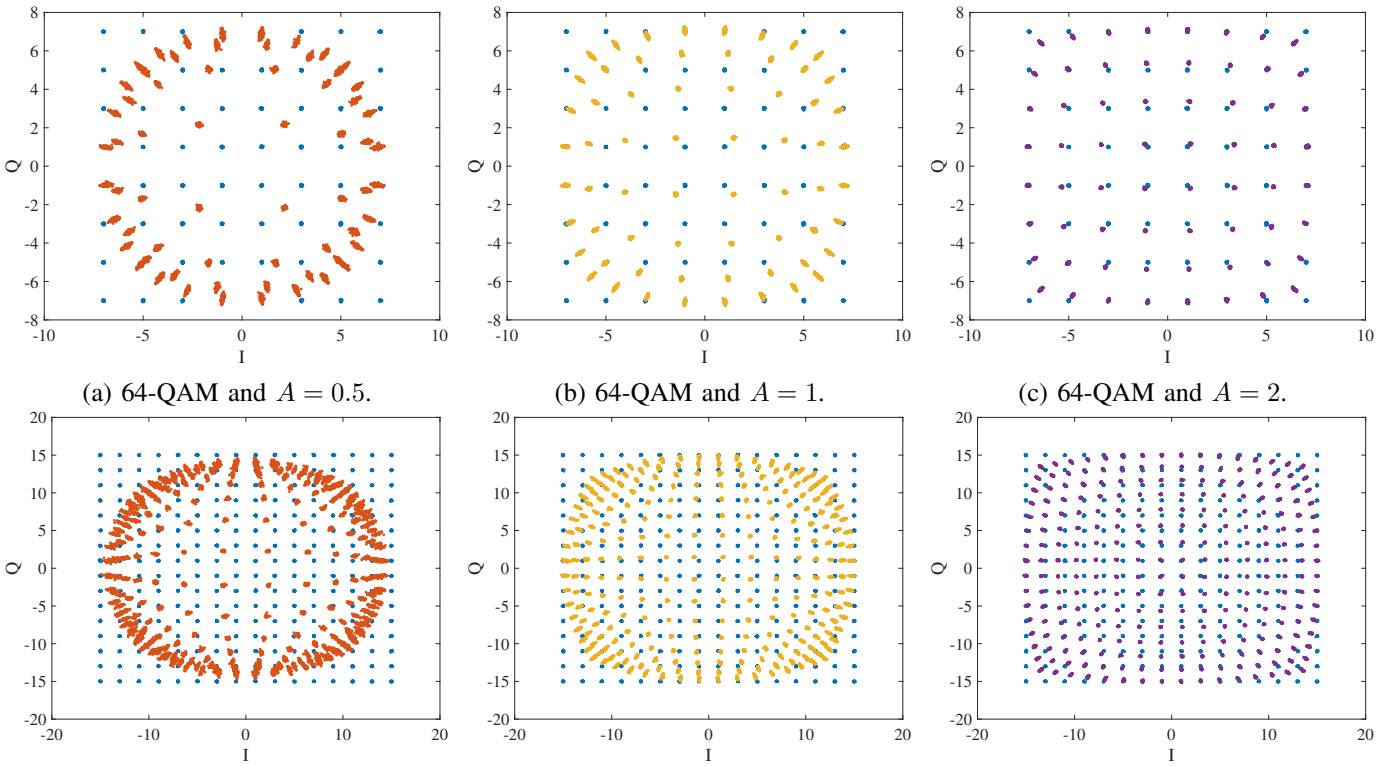

(a) 64-QAM and $A = 0.5$. (b) 64-QAM and $A = 1$. (c) 64-QAM and $A = 2$.

(d) 256-QAM and $A = 0.5$. (e) 256-QAM and $A = 1$. (f) 256-QAM and $A = 2$.

Fig. 5: Comparison of the decoded signal constellation at the BS in the uplink for 64-QAM and 256-QAM with a PA saturation of $A \in \{\text{Ideal}, 0.5, 1, 2\}$. The colors in the figures stand for – Ideal, – $A = 0.5$, – $A = 1.0$, and – $A = 2.0$.

[4] F. Rusek, D. Persson, B. K. Lau, E. G. Larsson, T. L. Marzetta, and F. Tufvesson, "Scaling Up MIMO: Opportunities and Challenges with Very Large Arrays," *IEEE Sig. Process. Mag.*, vol. 30, pp. 40–60, Jan. 2013.

[5] R. S. Chaves, E. Cetin, M. V. S. Lima, and W. A. Martins, "On the Convergence of Max-Min Fairness Power Allocation in Massive MIMO Systems," *IEEE Commun. Lett.*, vol. 24, pp. 2873–2877, Dec. 2020.

[6] R. S. Chaves, M. V. S. Lima, E. Cetin, and W. A. Martins, "User Selection for Massive MIMO under Line-of-Sight Propagation," *IEEE Open J. Commun. Soc.*, vol. 3, pp. 867–887, May 2022.

[7] R. S. Chaves, E. Cetin, M. V. S. Lima, and W. A. Martins, "Fading-ratio-based Selection for Massive MIMO Systems under Line-of-sight Propagation," *Wirel. Netw.*, vol. 28, pp. 3525—-3535, Jul. 2022.

[8] M. Matthaiou, O. Yurduseven, H. Q. Ngo, D. Morales-Jimenez, S. L. Cotton, and V. F. Fusco, "The Road to 6G: Ten Physical Layer Challenges for Communications Engineers," *IEEE Commun. Mag.*, vol. 59, pp. 64–69, Jan. 2021.

[9] E. Björnson, J. Hoydis, M. Kountouris, and M. Debbah, "Massive MIMO Systems With Non-Ideal Hardware: Energy Efficiency, Estimation, and Capacity Limits," *IEEE Trans. Inf. Theory*, vol. 60, pp. 7112–7139, Nov. 2014.

[10] C. Mollén, U. Gustavsson, T. Eriksson, and E. G. Larsson, "Out-of-band Radiation Measure for MIMO Arrays with Beamformed Transmission," in *IEEE International Conference on Communications*, (Kuala Lumpur, Malaysia), pp. 1–6, IEEE, May 2016.

[11] S. C. Cripps, *RF Power Amplifiers for Wireless Communications*. Artech House, second ed., 2006.

[12] B. Sridhar, N. K. Darimireddy, S. Sridhar, and S. Krishna, "Adaptive Filter Clipper-Based PAPR Reduction Techniques for Massive MIMO-OFDM," in *IEEE Wireless Antenna and Microwave Symposium*, (Visakhapatnam, India), pp. 1–5, IEEE, Feb. 2024.

[13] C. Yu, L. Guan, and A. Zhu, "Band-limited Volterra Series-based Behavioral Modeling of RF Power Amplifiers," in *IEEE/MTT-S International Microwave Symposium Digest*, (Montreal, Canada), pp. 1–3, IEEE, Jun. 2012.

[14] D. Morgan, Z. Ma, J. Kim, M. Zierdt, and J. Pastalan, "A Generalized Memory Polynomial Model for Digital Predistortion of RF Power Amplifiers," *IEEE Trans. Sig. Process.*, vol. 54, pp. 3852–3860, Oct. 2006.

[15] A. Saleh, "Frequency-Independent and Frequency-Dependent Nonlinear Models of TWT Amplifiers," *IEEE Trans. Commun.*, vol. 29, pp. 1715–1720, Nov. 1981.

[16] R. Rogalin, O. Y. Bursalioglu, H. C. Papadopoulos, G. Caire, and A. F. Molisch, "Hardware-impairment Compensation for Enabling Distributed Large-scale MIMO," in *Information Theory and Applications Workshop*, (San Diego, USA), pp. 1–10, IEEE, Feb. 2013.

[17] M. Yao, M. Sohul, R. Nealy, V. Marojevic, and J. Reed, "A Digital Predistortion Scheme Exploiting Degrees-of-Freedom for Massive MIMO Systems," 2018.

[18] N. D. Lahbib, M. Cherif, M. Hizem, and R. Bouallegue, "Power Amplifier Nonlinearities Effects on Massive MIMO Uplink Channel Estimation," in *International Conference on Software, Telecommunications and Computer Networks*, (Split, Croatia), pp. 1–6, IEEE, Sep. 2020.

[19] Y. Suzuki, H. Okazaki, T. Asai, and Y. Okumura, "Linearization Technologies for Power Amplifiers of Cellular Base Stations," in *IEEE International Symposium on Radio-Frequency Integration Technology*, (Melbourne, Australia), pp. 1–3, IEEE, Aug. 2018.

[20] X. Wang, S. Bi, X. Li, X. Lin, Z. Quan, and Y.-J. A. Zhang, "Capacity Analysis and Throughput Maximization of NOMA With Non-Linear Power Amplifier Distortion," *IEEE Trans. Wirel. Commun.*, vol. 23, pp. 18331–18345, Dec. 2024.

[21] S. O. Rice, "Mathematical Analysis of Random Noise," *The Bell System Technical Journal*, vol. 23, pp. 282–332, Jul. 1944.

[22] E. Björnson, J. Hoydis, and L. Sanguinetti, *Massive MIMO Networks: Spectral, Energy, and Hardware Efficiency*. Now Foundations and Trends, 2017.

[23] C. Rapp, "Effects of HPA-nonlinearity on 4-DPSK/OFDM-signal for a Digital Sound Broadcasting System," in *2nd European Conference on Satellite Communication*, (Liege, Belgium), pp. 179–184, Oct. 1991.

[24] R. Prasad, *OFDM for Wireless Communications Systems*. Artech, first ed., 2004.